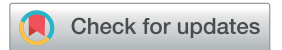
Journal of Materials Chemistry A



PAPER

View Article Online
View Journal | View Issue



Cite this: J. Mater. Chem. A, 2018, 6, 12708

Electrodeposited thin-film Cu_xSb anodes for Li-ion batteries: enhancement of cycle life *via* tuning of film composition and engineering of the film-substrate interface†

Electrodeposited Cu–Sb thin films on Cu and Ni substrates are investigated as alloy anodes for Li-ion batteries to elucidate the effects of both the film composition and substrate interactions on anode cycling stability and lifetime. Thin films of composition Cu_xSb (0 < x < 2) exhibit the longest cycle lifetimes nearest x = 1. Additionally, the Cu–Sb films exhibit shorter cycle lifetimes when electrodeposited onto Cu substrates when compared to equivalent films on Ni substrates. *Ex situ* characterization and differential capacity analysis of the anodes reveal that significant interdiffusion occurs during cycling between pure Sb films and Cu substrates. The great extent of interdiffusion results in mechanical weakening of the film–substrate interface that exacerbates film delamination and decreases cycle lifetimes of Cu–Sb films on Cu substrates regardless of the film's composition. The results presented here demonstrate that the composition of the anode alone is not the most important predictor of long term cycle stability; the composition coupled with the identity of the substrate is key. These interactions are critical to understand in the design of high capacity, large volume change materials fabricated without the need for additional binders.

Received 23rd February 2018 Accepted 19th May 2018

DOI: 10.1039/c8ta01798k

rsc.li/materials-a

1. Introduction

Informing design principles for next generation secondary batteries is a step toward achieving the high energy density and long cycle lifetime requirements of grid-scale energy storage and the electrification of transportation. In particular, alloy anodes for Li-ion and Na-ion batteries show promise for achieving higher energy densities by storing more working ions $(I^+ = Li^+, Na^+)$ per unit volume and mass than traditional intercalation anodes. The specific capacity of an active alloy material (A) is determined by the stoichiometry of the produced phase in the reversible alloy reaction:

$$A + \chi I^+ + e^- \leftrightarrow I_{\nu}A$$

Elements that have shown reasonable functionality as alloy anodes include but are not limited to Si, Sn, Sb, Al, and Mg for Li-ions³ and Sn, Sb, Ge, and P for Na-ions.^{1,4} However, these anodes typically exhibit very large volume changes upon cycling,

and hence demonstrate significant capacity fading within a few cycles that limit their lifetimes.

The capacity fade is commonly attributed to two coinciding and interacting failure modes:⁵

- (a) Uncontrolled formation of the surface-electrolyte-interface (SEI) layer and
 - (b) Mechanical instability of the active material.

The SEI is a heterogeneous layer that forms as electrolyte electrochemically decomposes on the anode surface during device cycling. The SEI layer can cause performance degradation and irreversible capacity loss by slowing, blocking, or consuming the working ions. Alloy anodes also undergo large volume changes during alloying and dealloying that can cause fracturing of the active material. Not only can the fracturing cause irreversible capacity loss as active material loses electrical connectivity with the rest of the electrode, it also degrades the existing SEI and exposes new surfaces of the electrode that result in additional SEI formation.^{3,6,7}

Strategies that successfully alleviate the mechanical instability of alloy anodes often times exacerbate deleterious effects of SEI formation. Structuring of the anode active material at nanoscale dimensions has proven to be effective at accommodating volume changes to prevent mechanical fracturing during cycling.⁸ However, the increased surface area of nanostructures results in greater amounts of SEI formation.^{9,10} Another approach is to use conversion type anodes that store working ions according to the following reaction:

^aDepartment of Chemistry, Colorado State University, Fort Collins, Colorado 80523, USA. E-mail: amy.prieto@colostate.edu

bLos Alamos National Laboratory, Los Alamos, New Mexico 87544, USA. E-mail: rkschulze@lanl.gov

[†] Electronic supplementary information (ESI) available. See DOI: 10.1039/c8ta01798k

where an inactive component M is extruded from the structure during alloying.7,11 While this conversion style chemistry can alleviate mechanical degradation of the active material by lessening the magnitude of volume change, exposing a fresh surface of extruded inactive component every cycle can lead to excessive SEI formation and degradation of battery performance.¹² Design strategies to mitigate the limited cycle lifetimes of alloy anodes must therefore concurrently address both the SEI formation and mechanical instability of anode materials.

The compound Cu₂Sb has been shown to be a promising conversion anode material, where its good cycling performance has been attributed to the reversibility exhibited during lithiation and delithiation. The compound reforms its original structure during alloying/dealloying cycles with lithium, likely due to structural relationships between Cu₂Sb, the fully lithiated Li₃Sb, and intermediate Li-Cu-Sb ternary phases. 13-15 Furthermore, Sb-based anodes have shown promise in Na-ion battery systems, 1,16-18 making the Cu-Sb system more widely relevant for next generation secondary batteries.

Building off of the wealth of literature on Cu-Sb anodes,19-22 our group has recently reported on the electrodeposition and cycle performance Cu-Sb anodes in Li-ion batteries in both thin film12,23 and nanowire array9 architectures. Producing the anodes by carefully tuned electrodeposition methods offers compositional control, conformal coverage, good mechanical adhesion, and by the nature of the technique, good electrical contact to the current collector, which eliminate the need for carbon additives and binders of traditional slurry anodes.23 Because the nature of the SEI on alloy/conversion anodes is known to be different than on graphite-based intercalation anodes,5 the absence of the carbon additives and binders allowed us to investigate the performance effects of SEI that are intrinsic to just the active material. By utilizing this strategy in a Cu-Sb nanowire-array anode with minimized mechanical instability but exaggerated SEI effects, we demonstrated that electrolyte additives can improve the stability of the SEI on Cu-Sb anodes.9

While the interplay of mechanical instability with the SEI at the anode-electrolyte interface is known to affect cycle performance, chemical and mechanical interactions between the active material and the current collector can also have significant effect on cycling stability of the anodes. Previous reports demonstrate that mechanical adhesion and cycle performance of electrodeposited Sn-based Li-ion anode thin-films can be improved by using textured instead of smooth Cu substrates. 24,25 Additionally, annealing of Sn-based thin film anodes causes interdiffusion between the active material and substrate, which can both improve or worsen cycling performance depending on the intermetallic phases formed.24-26 These types of substrate-interface interactions are especially important in electrodeposited anode materials where there is direct contact between the active material and current collector during electrochemically driven structural changes. Incomplete adhesion and incoherent interface development at a film-substrate interface can result in film delamination, which in a battery anode means electrical isolation from the current collector and an associated irreversible capacity loss.

Herein, we demonstrate enhancement of cycle lifetimes of Cu-Sb thin film anodes by controlling substrate-film interactions. First, using electrodeposited pure Sb films on Cu foil substrates we show that substrate-film interdiffusion forms Kirkendall-like voids that weaken the interface and exacerbate mechanical degradation and film delamination during cycling. Pure Sb films were chosen as a starting point to exaggerate volume expansion issues as well as to exaggerate the concentration gradient at the Sb-Cu interface. We then show that this degradation mode occurs in Cu-Sb films on Cu substrates regardless of their composition and how it can be eliminated to improve anode cycle lifetimes by using Ni foil substrates or Niblocking layers, where no substrate-film interdiffusion occurs. Additionally, while Sb metal and Cu₂Sb are commonly reported as Li-ion battery anodes, we show how cycle performance can be further improved using off-stoichiometric Cu_xSb (0 < x < 2) compositions that balance competing failure modes. While these design strategies are explored in our specific system, the principles of balancing failure modes are likely applicable to battery systems where different alloy anode materials and working ions are used.

2. Results and discussion

Electrodeposited Sb thin films cycle longer on Ni substrates than on Cu

As an initial measure of substrate type effects on the cycling of Sb based anodes, equivalent Sb films were electrodeposited to charge loadings of 702 mC cm⁻² (~440 nm approximate thickness) onto Cu and Ni foil substrates and used as-deposited in Li-ion half cells. Fig. 1A shows the retained reversible capacity of these anodes as measured by charge capacity relative to the initial capacity. The substantial capacity loss of the Sb film on the Cu foil (Sb@Cu) within 10 cycles indicates unstable cycling behavior and a relatively short cycle lifetime. The Sb film

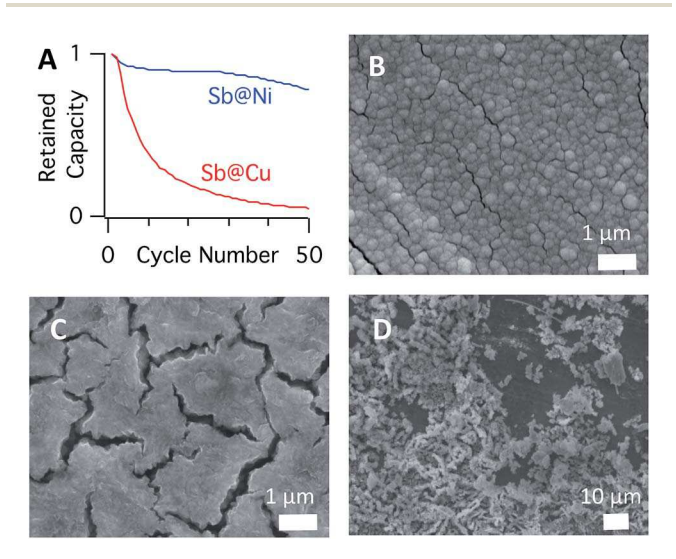


Fig. 1 (A) Cycle performance of equivalent Sb thin films on Cu and Ni metal substrates. SEM micrographs show Sb film morphology before cycling (B) and after cycling on a Ni substrate (C, D).

on the Ni foil (Sb@Ni) shows a comparatively lesser capacity decline beginning around 30 cycles, indicating a more stable cycling behavior and a longer cycle lifetime. Pre- and postcycling ex situ SEM imaging of the films identifies cracking and film delamination typical of alloy-anodes as the main cause of capacity loss and anode failure. The as-deposited films exhibit comparable surface morphologies on both the Cu and Ni foils (Fig. 1B), exhibiting uniform and conformal coverage while cracks indicate some internal stress of these films. After 50 cycles the Sb@Ni anode shows expanded cracks (Fig. 1C) and areas of delamination (Fig. 1D). Imaging of the Sb@Cu anode after 50 cycles was not possible because the film had totally delaminated from the Cu foil as a black powder during battery disassembly. Post-cycling observations of the thin films is consistent with commonly observed mechanical instability failure modes and seems to be exacerbated on the Cu foil substrates. To elucidate the effects of the substrate metal on the cycling stability of the Sb films, additional in situ and postcycling characterizations were performed.

2.2 Thin film Sb on Cu substrate converts to Cu₂Sb during cycling

To further investigate the cause for the drastic differences in cycle performance on Cu and Ni substrates for Sb films, thin film anodes of Sb@Cu and Sb@Ni with charge loadings of 228 mC cm $^{-2}$ (\sim 140 nm approximate thickness) were prepared and characterized using ex situ XRD before and after cycling. The thinner samples and fewer cycles lead to less severe degradation of the Sb@Cu anode, allowing for post-cycling characterization to be performed. Voltage-capacity traces for charge and discharge of the Sb@Cu anode (Fig. 2A) show an irreversible capacity loss above 1 V on the first discharge, lithiation plateaus between 0.5 and 1.0 V, and delithiation plateaus around 1 V, all of which are typical for Sb-based anodes. Differential capacity plots that more clearly display the anode electrochemistry (Fig. 2B) show evolution of the anode electrochemistry over 6 cycles. The (a) peaks in Fig. 2B are typical lithiation/delithiation potentials for Sb metal¹⁰ while the (b) peaks are typical of Cu₂Sb lithiation/delithiation potentials.27 The evolution of peaks from (a) to (b) indicates significant conversion of the Sb film to Cu₂Sb over only 6 cycles. Such a materials transformation from an amorphous Sb to a crystalline Cu₂Sb film is consistent with the pre- and post-cycling XRD (Fig. 2C). Ex situ Auger spectroscopy depth profiles of the pre- and post-cycled anodes confirms the interdiffusion of the Sb film with the Cu substrate (Fig. S1, ESI†).

There is no analogous conversion from Sb to a crystalline Ni–Sb intermetallic phase when cycling the Sb@Ni anode, as evidenced by voltage profiles typical of Sb and post-cycling XRD that shows only crystalline Sb reflections (Fig. S2, ESI†) during more than 10 cycles. The structural similarities between Li₃Sb, Li–Cu–Sb intermediates, and Cu₂Sb and the fast solid-state diffusion of Cu into Sb²⁸ is most likely what allows for the material transformation during cycling in the Sb@Cu but not the Sb@Ni anodes. The *ex situ* XRD of the Sb films additionally shows the pre-cycled material as a broad amorphous reflection around 29° and the post-cycled material contains evidence of

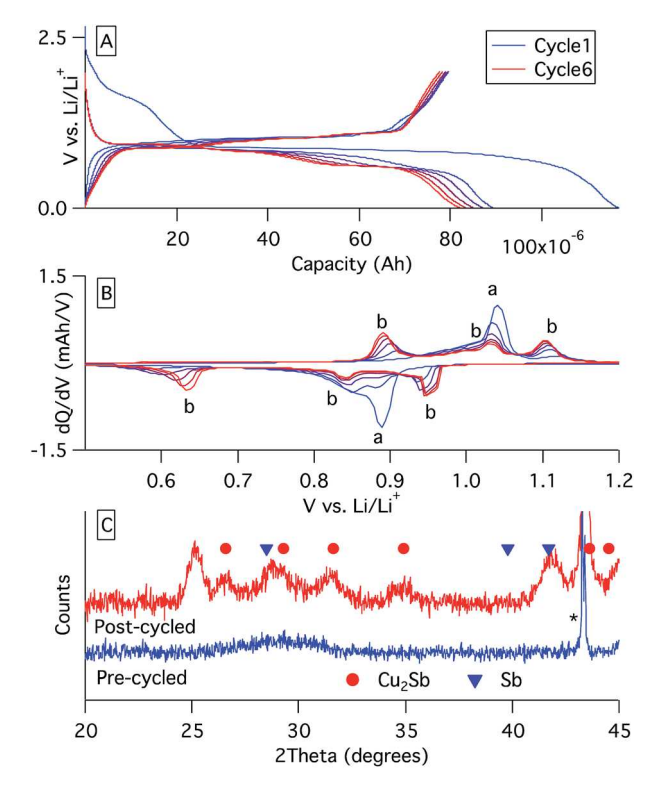


Fig. 2 Characterization of Sb@Cu anode cycled in a Li-ion battery: (A) charge—discharge curves for 6 cycles between 0.05–2 V vs. Li/Li⁺, (B) the corresponding differential capacity plots, (C) and *ex situ* XRD before and after cycling. The Cu substrate is marked by *.

 ${
m Sb_2O_5}$ with a Bragg reflection at 25° . The presence of oxygen through the full thickness of the films on both Cu and Ni substrates is confirmed by Auger spectroscopy (Fig. S1, ESI†). The presence of oxygen in the film and its amorphous nature may also play a role in the extent of Cu–Sb interdiffusion. Poor cycling stability of the Sb@Cu anode compared to the Sb film of the Sb@Ni anode could arise from the Cu–Sb composition formed from the interdiffusion. Variable composition ${\rm Cu}_x{\rm Sb}$ (0 < x < 2) films on Ni foils where the Cu : Sb ratio stays constant during cycling can be used to determine the effect of only composition on cycling stability.

2.3 Electrodeposited Cu_xSb thin film anodes show composition dependent cycle lifetimes

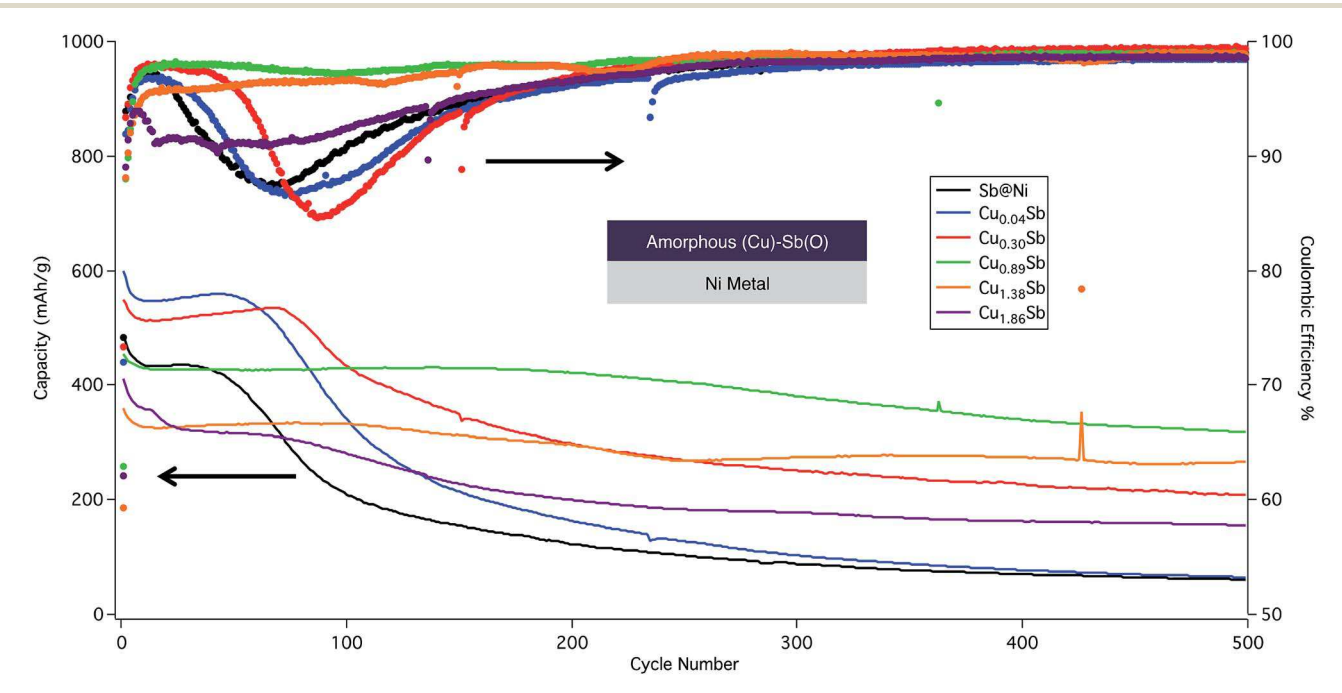
To investigate the dependency of cycling stability on film composition, thin film $\mathrm{Cu}_x\mathrm{Sb}$ (0 < x < 2) anodes were electrodeposited onto Ni foil substrates to a charge loading of 232 mC cm $^{-2}$ (\sim 110–140 nm approximate thickness). The film compositions were controlled by changing the concentration of CuCl_2 in the deposition solution and determined using EDS. Imaging using SEM of the as-deposited films shows similar surface morphology between films of different compositions and to the film in Fig. 1B. Analysis by EDS (Fig. S3, ESI†) indicates about 30–50 atom% oxygen in the films (which includes oxygen that is likely present in the SEI layer), and Auger spectroscopy depth profiling shows the oxygen is present through the full thickness of the films. The incorporation of $\mathrm{Sb}_2\mathrm{O}_3$ into electrodeposited

films of Sb has been previously reported,29 and has been shown to boost the lithium storage capacity and cycle lifetimes of the films through the partially reversible formation of Li₂O. While the oxygen content varies between the electrodeposited films, we believe the Cu: Sb ratio plays a more significant role in the reversible capacity and cycling stability of these films. Deposition of these films onto Ni foil substrates ensures that the Sb: Cu ratio of the films stays constant during cycling, unlike Sb@Cu anodes where Cu from the substrate can diffuse into the film during cycling. Fig. 3 shows the cycle lifetimes of the CuxSb@Ni anodes as measured by the specific delithiation capacity for each cycle.

Generally, the initial specific capacity of the anodes decreases with increasing Cu content, which is consistent with film compositions that have larger inactive component (Cu) to active component (Sb) ratios. There are exceptions to this trend that may arise from loading discrepancies between samples, such as in the case of the Sb-only Sb@Ni anode that falls far short of its theoretical maximum capacity of 660 mA h g^{-1} . Coulombic inefficiencies during electrodeposition give rise to overestimations of anode loading as determined via counting the charge passed during deposition. The disparity of the Sb@Ni anode capacity is attributed to a lower coulombic efficiency in a deposition solution without Cu2+ ions. This observation is consistent with our previous report of induced underpotential deposition of Cu₂Sb from aqueous solution.³⁰

Regardless of error in the specific capacity magnitude between anodes, examination of the capacities' evolution over many cycles gives insight about how the anode composition affects cycling stability. The anodes with low Cu contents exhibit first cycle coulombic efficiencies around ~70% while those with higher Cu contents have \sim 60% efficiency, suggesting the higher Cu contents results in more extensive SEI formation

on the first lithiation. Note that coulombic efficiency here refers to the ratio of current out/current in, and with these anodes we expect significant surface roughening (hence the observed increase in capacity over many cycles), leading to fresh surface exposed for SEI formation. The rising coulombic efficiencies and steep drops in specific capacities within the first few cycles of all compositions suggest that the SEI continues to form over the first few cycles. Additional steep drops in the specific capacities and dips to around 90% in coulombic efficiency at later cycles mark the regions of "anode failure" characterized by significant and rapid capacity loss as lithiated active material looses contact with the current collector. The number of cycles where such an anode failure region begins serves as a rough quantitative measure of that anode's cycling stability. Anode failure begins around 40 cycles for the Sb-only Sb@Ni anode where the main mechanism of capacity loss seems to be mechanical degradation and film delamination like seen in Fig. 1D. The beginning of anode failure is extended to around 50 and 70 cycles in the Cu_{0.04}Sb@Ni and Cu_{0.30}Sb@Ni anodes, respectively, which is expected as the inclusion of more inactive Cu in the film would better buffer volume changes and slow the mechanical degradation and delamination. At higher Cu concentrations, the films' specific capacities start out smaller but diminish to a lesser extent. The Cu_{0.89}Sb@Ni anode shows negligible capacity loss for around 150 cycles before slowly and steadily losing capacity. A similar behaviour is seen in the Cu_{1.38}Sb@Ni anode, though its capacity diminishes slightly around 100 cycles. The Cu_{1.86}Sb@Ni anode shows a capacity drop around cycle 20 before beginning another failure around 70 cycles. Overall, most capacity loss of the anodes is attributed to loss of active material by delamination, while slight increases in capacity may be a result of increased surface area from mechanical roughening that opens new lithiation/delithiation



Cycle performance of variable composition amorphous Cu-Sb thin films on Ni substrates.

avenues or results in additional SEI layer formation. Post-cycling EDS analysis (Fig. S3, ESI†) of the anodes shows significantly increased oxygen contents over the pristine anodes, which is consistent with substantial SEI formation and its oxidation upon exposure and storage in air before analysis.

Generally it seems that the anodes with the best cycling stability have compositions close to Cu₁Sb. This cycling behaviour is consistent with our recent report on Cu_xSb@Cu thin film anodes with compositions of 1 < x < 3 where the anode with x = 1 exhibits the best cycling stability.¹² At anode compositions where x > 1, the mechanisms that negatively impact cycling stability are two-fold. With increased Cu content, Li can become more easily trapped in the film by Cu-rich phases during delithiation. Additionally, greater amounts of Cu being repeatedly extruded and reincorporated during cycling result in repeated SEI formation on the newly exposed electroactive surfaces. At a composition near x = 1, we believe the impact of the above mechanisms of capacity loss to be minimized while maintaining enough Cu content for the anode to access Li-Cu-Sb intermediate phases during cycling. Access to these phases significantly alleviates mechanical stresses during cycling by allowing access to multiple lithiation and delithiation events that occur stepwise and at distinct potentials rather than the lithiation and delithiation events consolidated to relatively small voltage regions in Sb metal anodes. Additionally, the fully lithiated cubic Li₃Sb phase $(Fm\bar{3}m)$ is more structurally similar to the cubic Li-Cu-Sb intermediate phases $(F\overline{4}3m)$ than the rhombohedral Sb metal phase $(R\bar{3}mH)$. The structural similarities and stepwise reactions during lithiation and delithiation lessen the impact of the volume changes on the film's mechanical integrity. The access to the intermediate Li-Cu-Sb phases can be seen as the three lithiation and delithiation peaks

in the differential capacity plots, like those shown as the (b) peaks in Fig. 2B. The $Cu_{0.89}Sb@Ni$ and higher Cu concentration anodes show these peaks in the differential capacity plots (Fig. S4, ESI†), giving rise to generally better cycling stability than the anodes with lower Cu concentrations.

2.4 Thin film Cu–Sb anodes show substrate dependent cycle lifetimes

Given that anode compositions with some Cu content display better cycling stability than pure Sb metal on Ni substrates, Sb@Cu anodes may perform worse than the Sb@Ni anodes due to the process of Cu-Sb interdiffusion rather than a composition resulting from said interdiffusion. To test how filmsubstrate interactions affect cycling stability regardless of film composition in Li-ion half-cells, we electrodeposited and cycled variable composition Cu-Sb thin film anodes on both Cu and Ni substrates. For these particular anodes, we modified a previously reported deposition method to produce films of higher crystallinity and oxygen contents of about 10-30 atom% (Fig. S5-S7, ESI†). Changing the concentration of the Cu precursor in the deposition solution was used to vary the Cu: Sb ratio in the film. The anode films were all deposited to charge loadings of 228 mC cm⁻² (~110-140 nm approximate thickness). As such, varying coulombic inefficiencies between depositions contribute error to the specific delithiation capacities shown in Fig. 4, though examining the capacities over many cycles can be used to assess cycling stability. The first cycle coulombic efficiencies are generally lower in the anodes with higher Cu content, again suggesting more extensive SEI formation on the first lithiation with more Cu content in the anode. The lack of steep drops in capacity in the first few cycles

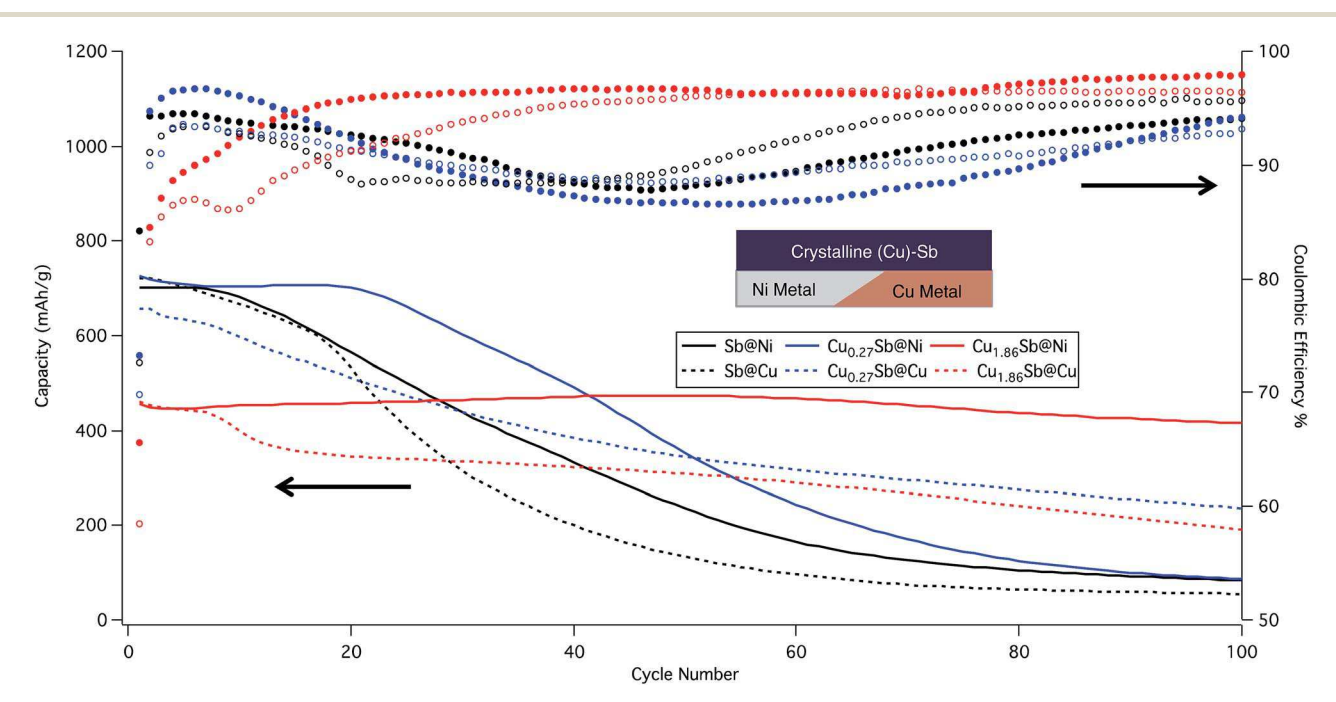


Fig. 4 Cycle performance of variable composition crystalline Cu–Sb thin films on both Ni (solid traces/filled dots) and Cu (dashed traces/open circles) substrates.

suggests the SEI forms faster on the crystalline films with lower oxygen content. Though compositions continuous across the complete Cu_xSb (0 < x < 2) range were not tested, anodes on the Ni substrates shown in Fig. 4 (solid traces) show better cycling stability with higher Cu contents, which is consistent with the composition effects on cycling stability discussed previously. The corresponding anodes of identical compositions but on Cu substrates (dashed traces) all exhibit anode failure features where steep drops in capacity and dips to ~90% coulombic efficiency occur before 30 cycles. These capacity drops on the Cu substrates that are relatively delayed on Ni substrates indicate that film-substrate interactions such as Cu-Sb interdiffusion may negatively impact cycling stability regardless of the film's composition. Post-cycling EDS analysis (Fig. S5, ESI†) of the anodes again shows significantly increased oxygen contents attributed to the exposure of formed SEI layers prior to analysis.

To determine if interdiffusion between Cu-Sb is a contributing factor to the poor cycling stability of the crystalline Cu-Sb@Cu anodes when compared to the crystalline Cu-Sb@Ni anodes, ex situ characterization and close examination of the cycling data was performed. Unlike the amorphous Sb@Cu anode discussed previously, post-cycling XRD of the crystalline Sb@Cu anode after 10 cycles (Fig. S7, ESI†) shows no crystalline Cu₂Sb reflections. This disparity suggests that the significant Cu-Sb interdiffusion in the amorphous Sb@Cu anode is driven by the amorphous nature of that film. While XRD does not indicate significant Cu-Sb interdiffusion is occurring during cycling of the crystalline Sb@Cu anodes, the differential capacity plot of the crystalline Sb@Cu anode over 10 cycles shows a small amount of lithiation/delithiation chemistry typical of Cu₂Sb as the circled peaks in Fig. 5A. The peaks indicate Cu-Sb interdiffusion is occurring, but likely localized

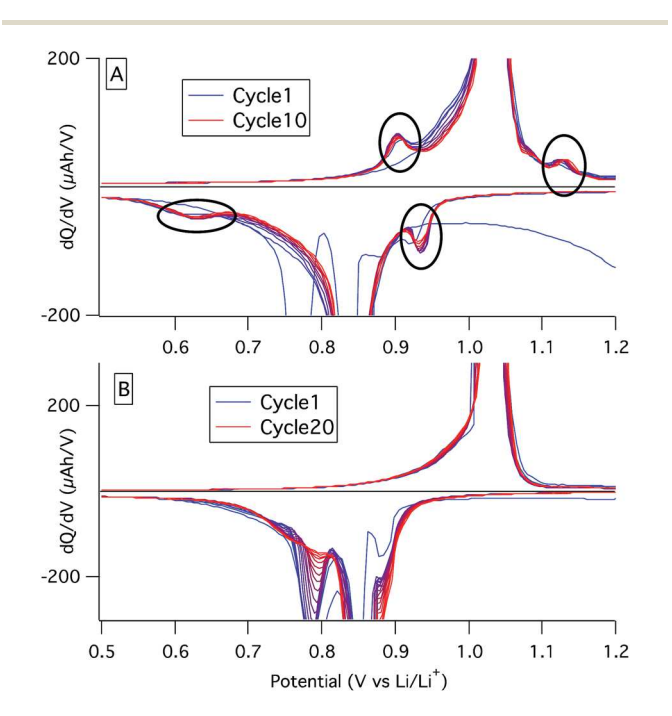


Fig. 5 Differential capacity plots of: (A) a crystalline-Sb@Cu anode and (B) a crystalline-Sb@Ni@Cu anode.

to the film-substrate interface where both Cu and Sb are present. It is this process of interface localized interdiffusion that may be responsible for the poor cycling stability of the anodes on Cu substrates.

2.5 Interdiffusion and void formation at film-substrate interfaces prevented by Ni blocking layers

We have shown that the use of Ni substrates prevents filmsubstrate interdiffusion and improves the cycling stability of these anodes. However, a Ni layer electrodeposited in between a Cu substrate and an electrodeposited Sb film can also achieve the same effect. Fig. 5B shows the differential capacity plot of a crystalline Sb@Ni@Cu anode where a Ni blocking layer is electrodeposited between the Sb film and Cu substrate. The plot shows no evidence of Cu₂Sb lithiation/delithiation chemistry indicating the Ni blocking layer effectively prevents even localized Cu-Sb interdiffusion. The cycle lifetime behavior of the Sb@Ni@Cu anode (Fig. S8, ESI†) closely matches that of an Sb@Ni anode with better cycling stability than an Sb@Cu anode. Similar Ni blocking layers are commonly used with microelectronic solders to prevent interdiffusion between Au-Cu and Sn-Cu contacts.31 At such contacts, a phenomenon known as the Kirkendall effect occurs when one metal diffuses into the other at a faster rate. This can cause the collection of structural vacancies into Kirkendall voids.32 Such voids can mechanically weaken contact interfaces and can result in device failures.33 Given that the Kirkendall effect has been reported in Cu-Sb systems,34 void formation at the film-substrate interface may be a mechanism for the exacerbated film delamination and poor cycling stability of Sb@Cu and Cu-Sb@Cu anodes.

By examining cross sectional SEM images, we see evidence of Kirkendall-like voids forming as a result of the Cu-Sb interface of Sb@Cu anodes. A ${\sim}500$ nm layer of Cu evaporated onto a Si wafer with a \sim 50 nm Cr adhesion layer was used as a substrate so that clean cross-sectional surfaces could be formed by cleaving the wafer. A crystalline Sb film was electrodeposited onto the Cu@Cr@Si as described in Section 2.4, and the Sb@Cu@Cr@Si anode was cycled a single time in a Li-ion halfcell between 0.5-2.0 V to prevent any lithiation of the Si substrate. Fig. 6A shows the cross-section of the cycled anode where voids have formed at the Cr-Cu interface. The voids can be more clearly visualized when the top Sb@Cu layers are delaminated from the Cr@Si substrate using adhesive tape. The underside of the delaminated Cu layer shown in Fig. 6B exhibits pitting that is reminiscent of pitting observed in an annealing study of Cu@Sb@Si samples.35

We believe the formation of these voids to be a result of interdiffusion at the Cu-Sb interface rather than any effect of the Cr@Si substrate. The voids collect at the Cr-Cu interface because it acts as a nucleation zone for vacancy coalescence and void formation in the Sb@Cu@Cr@Si anodes. EDS of the Cu layer underside shows no Cr signal, suggesting Cr-Cu interdiffusion is negligible during cycling and does not play a role in the Kirkendall void formation. To exclude effects of the CraSi substrate, an Sb@Cu anode was made and cycled for 100 cycles to totally delaminate the Sb film. The surface of the exposed Cu

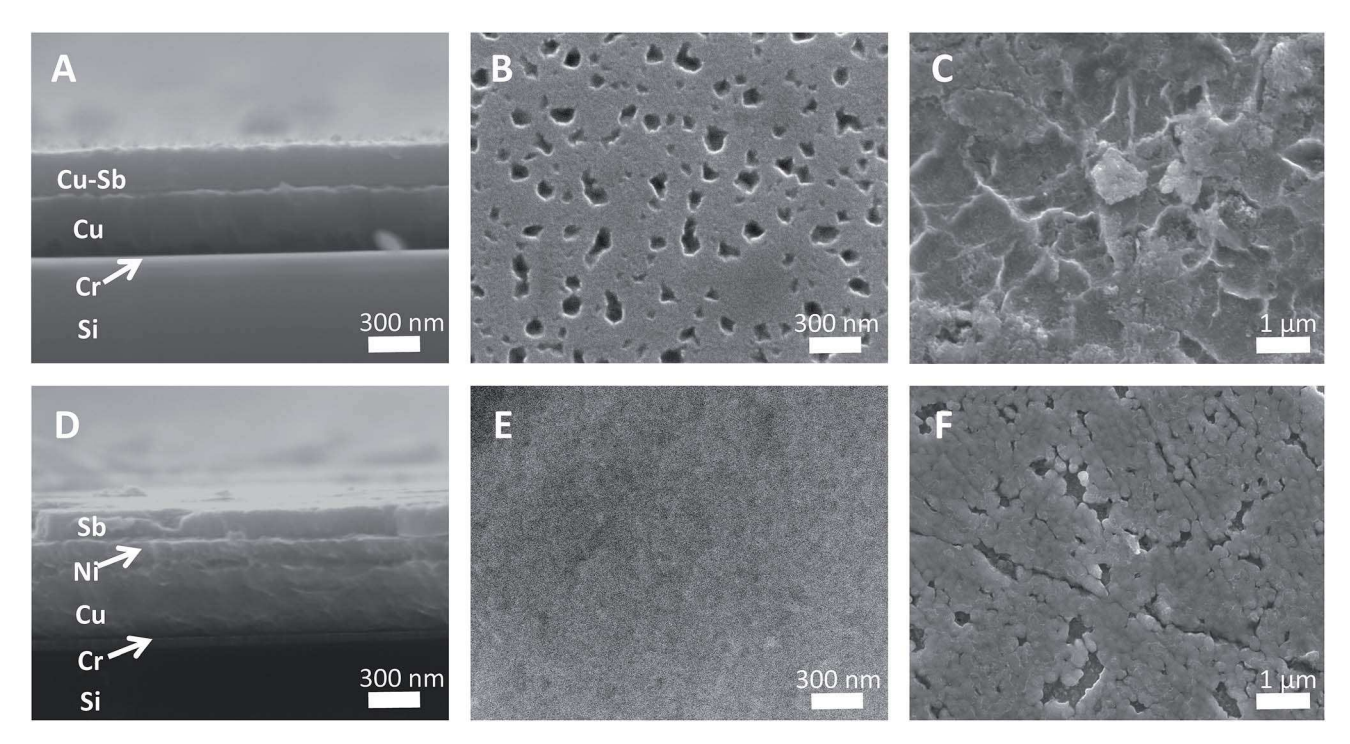


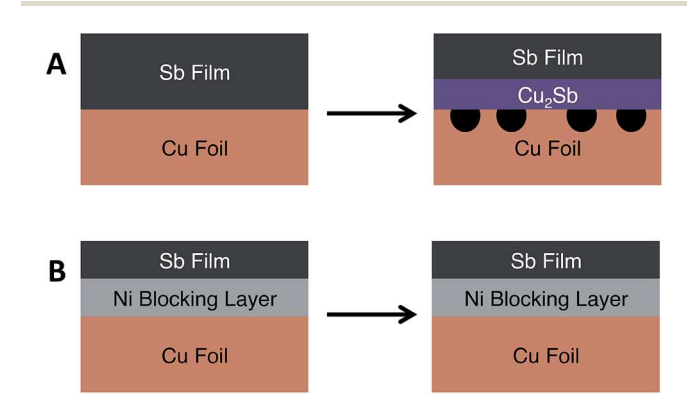
Fig. 6 SEM micrographs of cycled anode materials: (A) cross section of Sb@Cu@Cr@Si, (B) underside of Cu layer mechanically delaminated at the Sb@Cu—Cr interface, (C) Cu foil substrate surface where Sb delaminated during cycling, (D) cross section of Sb@Ni@Cu@Cr@Si, (E) underside of Cu layer mechanically delaminated at the Sb@Ni@Cu—Cr interface, (F) surface of Ni@Cu substrate where Sb delaminated during cycling.

foil is shown in Fig. 6C. Its corroded looking morphology suggests the same Kirkendall void formation occurs in the absence of Cr@Si and is a function of interdiffusion at the Cu–Sb interface only. Pitting and corroded Cu surfaces are also observed in cycled Cu₂Sb@Cu@Cr@Si and Cu₂Sb@Cu anodes. This observation indicates that the void formation behaviour also occurs in Cu-containing films on Cu substrates, probably due to the repeated extrusion and reincorporation of Cu during cycling.

To confirm that the voids form as a function of interdiffusion at the Cu-Sb interface, Ni blocking layers were used to prevent void formation in the cross sectional imaged anodes. Fig. 6D shows the cross section of an Sb@Ni@Cu@Cr@Si anode cycled a single time where a Ni blocking layer separates the Cu and Sb. There is no evidence of voids at the Cr-Cu interface, which is confirmed by the absence of pitting in the underside of the Cu layer (Fig. 6E) when delaminated by adhesive tape. Fig. 6F shows the exposed surface of a Ni blocking layer on a Cu foil after 100 cycles caused total film delamination of an Sb@Ni@Cu anode. Aside from small portions of the Ni blocking layer that delaminated with the Sb during cycling, the Ni blocking layer is intact and has its original surface morphology (Fig. S9, ESI†). Because the surface is not nearly as corroded at the one shown in Fig. 6C, the Ni is effectively preventing the Kirkendall void formation that results from Cu-Sb interdiffusion. These observations are consistent with the ability of a Ni substrate or blocking layer to prevent film-substrate interdiffusion, interface weakening, and concomitant decrease of cycling stability that is observed in Sb@Cu anodes.

2.6 Relevance of interdiffusion and interface weakening for Sn anodes, Na-ion batteries, and other devices

Scheme 1A shows a model of an Sb-Cu interface where the direct contact results in excessive interdiffusion, void formation, and interface weakening. While this process may be driven by repeated lithiation and delithiation cycles in a battery, it also occurs during static conditions at ambient temperature and a relevant rate. The delaminated underside of the Cu layer from an Sb@Cu@Cr@Si anode evolves from a pristine non-pitted surface (like Fig. 6E) immediately after deposition to a pitted surface (like Fig. 6B) after only a single day of being stored under vacuum. An analogous pitting process is observed at ambient temperature in electrodeposited Sn@Cu@Cr@Si anodes. The pitting from Sn-Cu contact is consistent with



Scheme 1 Cross sectional models of Sb thin films on Cu substrates: (A) crystalline-Sb@Cu and (B) crystalline-Sb@Ni@Cu.

previous reports of Kirkendall void formation at those interfaces³⁶ indicating Sn based anodes could also exhibit substrate dependent cycle lifetimes if interdiffusion between the film and substrate results in Kirkendall voids localized to the interface. Scheme 1B illustrates how a Ni blocking layer between Cu and Sb prevents interdiffusion and void formation, thus producing better cycling stability. The Ni blocking layer also prevents interdiffusion between Sn and Cu layers at ambient temperature as indicated by the absence of pitting on a delaminated Sn@Ni@Cu undersurface. Thus, Ni blocking layers have the potential to prevent Kirkendall void formation in any device where Sb@Cu or Sn@Cu contacts require mechanical stability, such as Na-ion batteries. More generally, interfacial layers that prevent or slow interdiffusion enough to prevent Kirkendall void formation can enhance the mechanical stability of that interface.

3. Conclusions

To help achieve the longer cycle lifetimes required for realization of high energy density Li-ion batteries, we have presented multiple strategies for improving cycling stability in Cu-Sb based anodes. Electrodeposition of Cu-Sb thin films onto metal foil substrates from aqueous solution is a facile anode production method where composition of the deposited film is easily controlled. We have shown that for thin films of $Cu_{2-x}Sb$ (0 < x < 2), optimal cycling stability is achieved near a composition of x = 1. This off-stoichiometric composition allows access to the Li-Cu-Sb ternary phases that improve cycling stability, while minimizing the amount of Cu that may cause excessive SEI growth when repeatedly extruded.

We have also shown how interdiffusion between Cu-Sb thin film anodes and Cu foil substrates during ambient temperature storage or cycling results in the formation of Kirkendall voids at the interface. The presence of the voids weakens the interfaces, exacerbated film delamination, and results in diminished cycling stability of any film composition on a Cu substrate. The lack of any analogous interdiffusion and weakening at Ni interfaces results in improved cycling stability of Cu-Sb films on Ni foil substrates. While interdiffusion can benefit cycling stability by forming intermetallic compositions, we propose the appearance of Kirkendall voids, especially when concentrated at an interface, to be a simple empirical threshold of when interdiffusion occurs to too great of an extent, or too quickly. These strategies for improving cycling stability can be generalized as design considerations for Li-ion and Na-ion batteries:

- (a) Electrodeposition of anodes allows access to offstoichiometric compositions that may outperform pure metal or intermetallic phases.
- (b) Interdiffusion that results in the formation of voids, especially when concentrated at interfaces, results in decreased cycling stability.
- (c) Blocking layers such as Ni provide a facile solution for preventing undesired interdiffusion that could form voids and weaken interfaces.

Experimental

Anode electrodeposition

The thin film anodes were electrodeposited using a Gamry Reference 3000 potentiostat. Depositions were performed using a Cu foil (McMaster Carr, 99.0% Cu) or Ni foil (Sigma-Aldrich, >99.9% Ni) substrate working electrode, platinum mesh counter electrode (McMaster Carr, Alloy 316 mesh), and a saturated calomel (SCE) reference electrode. Foil substrates were cleaned in a concentrated HNO3 solution for 30-60 seconds followed by rinsing in Millipore water and drying. The substrate foils were then masked with Kapton tape or a rubber gasket pressed to the metal surface to define a known area for electrodeposition on one side of the substrate. All electrodepositions were performed at ambient temperature between 21 and 24 °C. To minimize variability in the material loading and thicknesses between anode films to be compared, the amount of electrodeposited material was monitored via coulometry. By doing so the depositions could be normalized to a given amount of charge passed per unit area, what we herein refer to as the "charge loading" and given in units of mC cm⁻².

Anode deposition solutions used in Sections 2.1, 2.2, and 2.3 were prepared by first dissolving 1, 5, 14, 20, or 30 mM CuCl₂-·2H₂O (Sigma-Aldrich, dihydrate, 99+%) in a solution of 200 mM sodium gluconate (Sigma, >99%) in Millipore water (18.2 Mohm). Once completely dissolved, 30 mM SbCl₃ (Sigma-Aldrich, anhydrous, >99.0%) was dissolved in the solution and the resulting aqueous solutions were then titrated to a pH of 6.0 using a concentrated NaOH solution. Depositions from this solution were done potentiostatically at -1.60 V vs. SCE.

Anode deposition solutions used in Sections 2.4, 2.5, and 2.6 were prepared by first dissolving 25 mM Sb₂O₃ (Sigma-Aldrich, nano-powder, >99.9%) in a solution of 400 mM citric acid (Sigma-Aldrich, >99.5%) in Millipore water (18.2 Mohm) by mixing at 60 °C for at least 12 hours. Once the Sb₂O₃ was completely dissolved, 5, 40, or 80 mM Cu(NO₃)₂·2.5H₂O (Sigma-Aldrich, >99.99%) was added and the solution was slowly titrated to a pH of 6.0 by addition of a concentrated KOH solution. Depositions from this solution were done potentiostatically at -1.05 V vs. SCE.

The Ni blocking layers used in Sections 2.5 were deposited from a previously reported Ni plating bath.³⁷ Briefly, the bath is an aqueous solution of 280 g L⁻¹ NiSO₄·6H₂O, 45 g L⁻¹ NiCl₂-·6H₂O, 17 g L⁻¹ citric acid, 2 g L⁻¹ sodium saccharin, 0.2 g L⁻¹ 2-butyne-1,4-diol, titrated to a pH of 3.0. The Ni blocking layers were deposited onto the substrates from this solution potentiostatically at -1.0 V vs. SCE for 60 seconds each. The coated substrates were then rinsed with Millipore water before being used as substrates for the Cu-Sb anodes.

4.2 Scanning electron microscopy, energy-dispersive X-ray spectroscopy, X-ray diffraction, and Auger depth profiling

Scanning electron microscopy (SEM) analyses were done using the JEOL JSM-6500F microscope. Energy-dispersive X-ray spectroscopy (EDS) was done at 1k× magnification at three different spots to obtain an average film composition. Preparation of cross-sectional samples was done by scoring the back of the Si

substrate with a diamond scribe, then cleaving the substrate and deposited film immediately before imaging. Powder X-ray diffraction (PXRD) measurements were done using a Bruker D8 Discover DaVinci powder X-ray diffractometer. Auger spectroscopy and the Auger sputter ion depth profiles were obtained using a Physical Electronics 5600ci multi-technique surface analysis system. Auger spectroscopy and depth profiles were acquired with 5 keV primary electrons in spot analysis mode (<1 μ m diameter spot size) on a uniform blank location on the plated films. 4 keV Ar ions were used in the sputter profile analysis with sputter rate calibration on SiO₂ at 2.0 nm per minute erosion rate. In order to determine relative atomic concentrations from the Auger data, the following sensitivity factors determined for the system were used: O (0.296), Cu (0.307), Sb (0.704).

4.3 Li-ion half-cell cycling

The electrochemical activity of thin film anodes was studied using two electrode Swagelok cells. The anodes did not require any additives or binders, as the active material was directly deposited onto the Cu foil. Circular disks of 1/2 inch diameter were punched from the deposited thin films and used as working electrodes in Swagelok cells assembled in an argon atmosphere glove box. Li metal was used as the reference and counter electrode. The electrolyte used was BASF Selectilyte Sample Series A6 (a mixture of diethyl carbonate, dimethyl carbonate, lithium tetrafluoroborate, and other minor additives), which was absorbed into a Whatman glass filter sandwiched between two polymer separators in between the electrodes. The assembled cells were allowed to rest for at least 12 hours before cycling in order to reach a steady state open circuit voltage (OCV). The battery cells were galvanostatically cycled at ambient temperature using an Arbin Instruments battery tester. The cells were all cycled at a rate of C/5 between 0.01 V and 2.0 V vs. Li/Li⁺ unless specified otherwise. The current densities for a C/5 rate and the specific anode loadings were calculated using the charge loading measured during electrodeposition and the fraction of active component (Sb) as determined by EDS. Before post-cycling analysis, the cells were held at 2.0 V vs. Li/Li⁺ until current became negligible to ensure complete delithiation of the active material. The cells were then disassembled in air and the anode films rinsed with ethanol and dried before ex situ SEM and PXRD.

Conflicts of interest

There are no conflicts to declare.

Acknowledgements

The authors thank Dr Pat McCurdy (Central Instrumentation Facility) for assistance with the SEM-EDS. This work was supported through the NSF SSMC program (SSMC-1710672).

Notes and references

1 J.-Y. Hwang, S.-T. Myung and Y.-K. Sun, *Chem. Soc. Rev.*, 2017, 334, 928.

- 2 J. B. Goodenough, Energy Storage Materials, 2015, 1, 158-161.
- 3 M. N. Obrovac and V. L. Chevrier, *Chem. Rev.*, 2014, **114**, 11444-11502.
- 4 D. Kundu, E. Talaie, V. Duffort and L. F. Nazar, *Angew. Chem., Int. Ed.*, 2015, **54**, 3431–3448.
- 5 M. R. Wagner, P. R. Raimann, A. Trifonova, K. C. Moeller, J. O. Besenhard and M. Winter, *Electrochem. Solid-State Lett.*, 2004, 7, A201–A205.
- 6 M. Ebner, F. Marone, M. Stampanoni and V. Wood, *Science*, 2013, 342, 716–720.
- 7 D. Larcher, S. Beattie, M. Morcrette, K. Edström, J. C. Jumas and J.-M. Tarascon, *J. Mater. Chem.*, 2007, 17, 3759–3772.
- 8 C. K. Chan, H. Peng, G. Liu, K. McIlwrath, X. F. Zhang, R. A. Huggins and Y. Cui, *Nat. Nanotechnol.*, 2008, 3, 31–35.
- 9 E. D. Jackson and A. L. Prieto, ACS Appl. Mater. Interfaces, 2016, 8, 30379–30386.
- 10 M. He, K. Kravchyk, M. Walter and M. V. Kovalenko, *Nano Lett.*, 2014, 14, 1255–1262.
- 11 C. M. Ionica, P. E. Lippens, J. O. Fourcade and J. C. Jumas, *J. Power Sources*, 2005, **146**, 478–481.
- 12 E. D. Jackson, J. M. Mosby and A. L. Prieto, *Electrochim. Acta*, 2016, 214, 253–264.
- 13 L. Fransson, J. T. Vaughey, R. Benedek, K. Edström, J. O. Thomas and M. M. Thackeray, *Electrochem. Commun.*, 2001, 3, 317–323.
- 14 S. Matsuno, M. Noji, T. Kashiwagi, M. Nakayama and M. Wakihara, J. Phys. Chem. C, 2007, 111, 7548–7553.
- 15 S. Matsuno, M. Noji, M. Nakayama, M. Wakihara, Y. Kobayashi and H. Miyashiro, J. Electrochem. Soc., 2008, 155, A151-A157.
- 16 E. D. Jackson, S. Green and A. L. Prieto, ACS Appl. Mater. Interfaces, 2015, 7, 7447–7450.
- 17 L. Baggetto, E. Allcorn, A. Manthiram and G. M. Veith, *Electrochem. Commun.*, 2013, 27, 168–171.
- 18 A. Darwiche, C. Marino, M. T. Sougrati, B. Fraisse, L. Stievano and L. Monconduit, J. Am. Chem. Soc., 2012, 134, 20805–20811.
- 19 H. Bryngelsson, J. Eskhult, L. Nyholm and K. Edström, *Electrochim. Acta*, 2008, **53**, 7226–7234.
- 20 D. Applestone, S. Yoon and A. Manthiram, *J. Mater. Chem.*, 2012, **22**, 3242–3247.
- 21 T. Yang, H. Wang, J. Xu, L. Wang, W.-C. Song, Y. Mao and J. Ma, *RSC Adv.*, 2016, **6**, 78959–78962.
- 22 E. Allcorn and A. Manthiram, *ACS Appl. Mater. Interfaces*, 2014, **6**, 10886-10891.
- 23 J. M. Mosby and A. L. Prieto, J. Am. Chem. Soc., 2008, 130, 10656–10661.
- 24 J. Park, S. Rajendran and H. Kwon, *J. Power Sources*, 2006, **159**, 1409–1415.
- 25 N.-R. Shin, Y.-M. Kang, M.-S. Song, D.-Y. Kim and H.-S. Kwon, *J. Power Sources*, 2009, **186**, 201–205.
- 26 N. Tamura, R. Ohshita, M. Fujimoto, S. Fujitani, M. Kamino and I. Yonezu, *J. Power Sources*, 2002, **107**, 48–55.
- 27 M. Morcrette, D. Larcher, J. M. Tarascon, K. Edström, J. T. Vaughey and M. M. Thackeray, *Electrochim. Acta*, 2007, **52**, 5339–5345.
- 28 R. Halimi and A. Merabet, Surf. Sci., 1989, 223, 599-606.

- 29 H. Bryngelsson, J. Eskhult, L. Nyholm, M. Herranen, A. Oscar Alm and K. Edström, Chem. Mater., 2007, 19, 1170-1180.
- 30 J. M. Mosby, D. C. Johnson and A. L. Prieto, J. Electrochem. Soc., 2010, 157, E99-E105.
- 31 M. Paunovic, P. J. Bailey, R. G. Schad and D. A. Smith, J. Electrochem. Soc., 1994, 141, 1843-1850.
- 32 D. Kim, J.-H. Chang, J. Park and J. J. Pak, J. Mater. Sci.: Mater. Electron., 2011, 22, 703-716.
- 33 T. S. Huang, H. W. Tseng, Y. H. Hsiao, C. H. Cheng, C. T. Lu and C. Y. Liu, Electrochem. Solid-State Lett., 2011, 14, H393-H394.
- 34 K. Hoshino, Y. Iijima and K. Hirano, Trans. Jpn. Inst. Met., 1981, 22, 527-534.
- 35 M. Nasser, B. Mokhtar, B. Mahfoud, R. Mounir, Z. Fouzia and B. Chaouki, Mater. Technol., 2012, 46, 139-144.
- 36 J. M. Park, S. H. Kim and M. H. Jeong, Jpn. J. Appl. Phys., 2014, 53, 05HA06.
- 37 T. Doi, K. Mizumoto, S. Tanaka and T. Yamashita, Met. Finish., 2004, 102, 26-35.